Thin film electrodes from Pt nanorods supported on aligned N-CNTs for proton exchange membrane fuel cells

Peter Mardle[a], Xiaochao Ji[b], Jing Wu[b], Shaoliang Guan[c,d], Hanshan Dong[b], Shangfeng Du[a],

[a] *School of Chemical Engineering, University of Birmingham, Edgbaston, Birmingham, B15 2TT, UK*
[b] *School of Metallurgy and Materials, University of Birmingham, Edgbaston, Birmingham, B15 2TT, UK*
[c] *School of Chemistry, Cardiff University, Cardiff, CF10 3AT, UK*
[d] *HarwellXPS – The EPSRC National Facility for Photoelectron Spectroscopy, Research Complex at Harwell (RCaH), Didcot, Oxon, OX11 0FA, UK*

ARTICLE INFO

ABSTRACT

The enhanced performance of carbon nanotubes (CNTs) over carbon black as a catalyst support and the out-standing catalytic activities of one-dimensional (1D) Pt nanostructures endow them big potential for applications in fuel cells. However, the research has been mainly focused on the materials, and a combination of both 1D Pt nanostructures and CNTs to fabricate practical high power performance fuel cell electrodes still remains a challenge. In this work, we demonstrate catalyst electrodes from Pt nanorods grown on aligned nitrogen doped CNTs for proton exchange membrane fuel cell (PEMFC) applications. Short Pt nanorods are grown on CNTs deposited directly on 16 cm^2 carbon paper gas diffusion layers (GDLs) via plasma enhanced chemical vapour deposition (PECVD) and nitrided using active screen plasma (ASP) treatment, which are directly employed as cathodes for H_2/air PEMFCs. The thin open catalyst layer effectively enhances mass transfer performance and, with a less than half of the Pt loading, 1.23 fold power density is achieved as compared with that from com-mercial Pt/C catalysts. A better durability is also confirmed which can be attributed to the good structure stability of nanorods and the enhancement effects from the N-CNT support.

1. Introduction

Proton exchange membrane fuel cells (PEMFCs) are receiving ever increasing attention for automotive applications due to their high energy efficiency and less harmful pollutants emitted. However, while scale up of current technologies is pushing the applicability of PEMFCs, higher power performances are required to ultimately reduce the precious metal loading for a given PEMFC power scale [1]. Efforts in past decades have focused on improving catalytic activities of Pt based catalysts and reducing the over-potential for the oxygen reduction reaction (ORR) at cathodes [2]. To this end great improvements have been made with recently reported jagged Pt nanowires demonstrating an ultra-high mass activity of 13.6 A mg_{Pt}^{-1}, 31 fold higher than 2020 target, 0.44 A mg_{Pt}^{-1}, defined by the U.S Department of Energy [3]. Considering the big disparity in the performance of novel catalysts evaluated by half-cell electrochemical measurement in liquid acid electrolytes and within the membrane electrode assembly (MEA) in single cell tests [4], there is still big challenge to apply these novel catalyst nanostructures to fabricate fuel cell electrodes with high power performance to reduce the Pt loadings for minimal stack cost [1].

In light of the drive to more active ORR catalysts, alternatives to the conventional carbon black catalyst supports have been much considered [5]. Carbon nanotubes (CNTs) and graphene are two carbonaceous supports that have shown to improve the catalytic activity and stability of the supported Pt catalysts in comparison to mesoporous counterparts through enhanced electrical conductivity and metal-support interaction [6–8]. One of the inhibiting factors of such supports, asides from the difficulty in synthesis scale up, is that such pristine surfaces do not lend themselves well to the deposition of metal catalyst particles. Through surface functionalization with surface organic groups [9], metallic seeds [10,11] or heteroatom dopants [12,13], suitable anchoring sites can be provided, with additional benefits of further enhancements to the catalytic activity of the surface catalyst particles. Compared to the conventional acid treatment which can ne-gatively alter the mechanical and electronic properties of carbonaceous structures [14], heteroatom functionalization can provide additional catalytic enhancements and catalyst stability [15–18]. An additional advantage is that the use of heteroatoms to dope a carbon surface has also been shown to improve the catalytic activity of a supported metal catalyst through the change of the metal's d-band electronic structure

[19]. In particular, nitrogen doping (N-doping) can not only increase the binding energy of precious metals to a substrate, but it can also provide catalytically active carbon sites on an otherwise pristine surface [12,20].

Comparing with graphene, CNTs do not suffer from the serious is-sues caused by the aggregation and stacking of the graphene nanosheets in real fuel cells [21,22], and hence Pt coated CNTs have shown good performance in working fuel cells when the end application is well considered. For example, Tang et al used a thermal chemical vapour deposition (CVD) technique to grow a layer of CNTs on carbon paper and subsequently sputter coated Pt nanoparticles onto the surface [23]. Aligned arrays of CNTs were also achieved through CVD on quartz or aluminium substrates, which once transferred onto the Nafion electro-lyte membrane during MEA fabrication, show promising PEMFC per-formance [24,25]. Improved performance at high current densities was attributed to the ordered arrangement of the CNTs allowing effective gas and ion transportation, in addition to improved water management resulting from the hydrophobicity of CNTs.

Additionally 1D Pt nanostructures have shown enhanced perfor-mance compared to commercial catalysts at high current densities due to their regular alignment and increased catalytic activity [26,27]. The increase in catalytic activity comes primarily from the preferential growth in the < 111 > crystallographic plane thus exposing highly crystalline surface facets [28]. The combination of 1D Pt nanostructures and novel carbonaceous supports have therefore shown much improved catalytic performance although their promise has not yet been realised in practical fuel cells [29].

There is therefore space for a scalable synthetic technique of ad-vanced Pt nanostructures supported on N-doped CNTs where not only high activities can be exhibited but also good fuel cell power perfor-mance. In this work, we demonstrate the growth of CNTs directly onto gas diffusion layer (GDL) substrate by a plasma enhanced CVD (PECVD) approach, followed by N-doping achieved through active surface screen plasma (ASP) treatment, which has been previously employed for the functionalisation of carbon nanofibers [30] and even the GDL surface [31]. Short Pt nanorods are then grown onto the N-CNTs using a simple formic acid (HCOOH) based approach. The fabricated Pt/N-CNT gas diffusion electrodes (GDEs) are used directly as cathodes and tested in single H_2/air and H_2/O_2 PEMFCs and compared to commercial Pt/C electrodes, evaluating the impact that the N-CNT support has on the catalytic properties of the Pt nanorods and the role that the porous catalyst layer structure has on the mass transport of reactant gases.

2. Experimental

2.1. Materials

H_2PtCl_6 (8 wt% in water), HCOOH (≥ 95%), isopropyl alcohol (IPA) and ethanol (EtOH) were purchased from Sigma-Aldrich, UK. 10 wt% Nafion® solution (D1021) was obtained from Ion Power Inc., Germany. All H_2O was deionised using a Millipore water system (18 MΩ). Sigracet 39 BC GDLs were purchased from Fuel Cell Store, USA. A commercial Pt/C catalyst was used as a benchmark (45.9 wt$_{Pt}$%, TEC10E50E, Tanaka KikinzokuKogyo K. K. (TKK)). GDEs with 0.4 mg$_{Pt}$ cm^{-2} were acquired from Johnson Matthey (JM), UK and used as anodes for all MEAs.

2.2. N-CNT growth on the GDL surface

For the low temperature growth of carbon nanotubes, an active screen was set up on top of the samples during the growth process. The schematic diagram of the active screen settings within the PECVD system is shown in Fig. 1. Two 316SS active screen lids were put on top of the samples. The Sigracet 39 BC GDL was loaded onto the bottom worktable with the 10 mm separation between the lid and the sample.

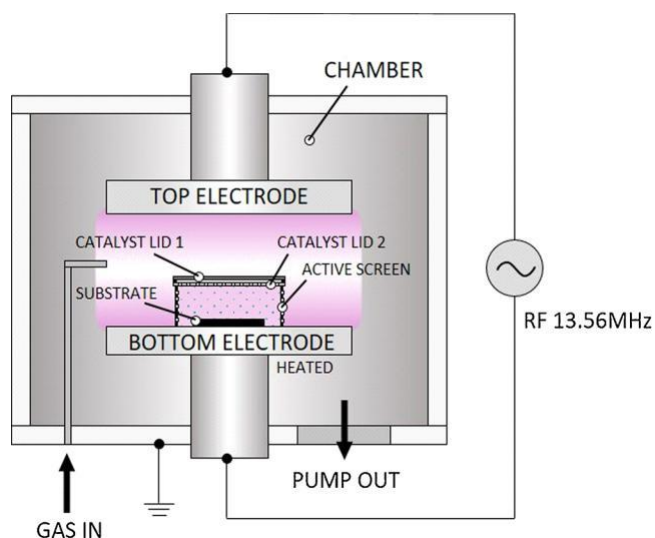The processes of the synthesis of CNTs are described as follows:

Fig. 1. Schematic diagram of the active screen settings to synthesize CNTs with P500 + PECVD system.

Firstly, the chamber was pumped down to a base pressure of 1×10^{-5} mbar to avoid the interference of the residual air. After that, the sam-ples were heated to 320 °C. Gas mixtures of Ar and H_2 were subse-quently fed into the chamber with flow rates of 50 sccm and 30 sccm respectively. The plasma was then turned on with a radiofrequency (RF) power of 300 W to clean the GDL surface. The cleaning process continued for 10 min. When the working temperature had stabilized, C_2H_2 gas was fed into the chamber as the carbon source at a flow rate of 5 sccm. During the growth process, C_2H_2 gas was diluted by Ar (50 sccm) and H_2 (20 sccm). The deposition was carried out with gas pressure of 1 mbar and working power of 30 W for 30 min. After the deposition, the power was shut down and C_2H_2 gas was stopped but exposure to the ambient of Ar and H_2 (50 sccm and 20 sccm, respec-tively) which was maintained during the cooling process down to room temperature. After the growth of CNTs, the CNT GDL was nitrided by N_2 plasma in an ambient of N_2 and H_2 (25% and 75%) at 200 °C for 10 min to obtain the N-CNT GDL.

2.3. Pt deposition

Pt deposition on the N-CNT GDLs was accomplished by the fol-lowing simple HCOOH reduction approach: the N-CNT GDL was wetted with H_2O and IPA before transferring to a petri-dish where a solution of 168 μL H_2PtCl_6 (8 wt% solution) in 8 mL H_2O was added. 530 μL of HCOOH was then added and the sample was left to react at 40 °C for 72 h followed by washing with H_2O and IPA. The Pt/N-CNT GDL was then dried in the oven at 60 °C and used directly as gas diffusion elec-trodes (GDEs) for fuel cell test.

2.4. Physical characterisation

Scanning electron microscopy (SEM) analysis was conducted on the representative GDEs using a Jeol 7000 F SEM with accelerating voltage 20 kV. Transmission electron microscopy (TEM) imaging was per-formed with a Jeol 2100 TEM, UK, with an accelerating voltage of 200 kV. The samples were prepared from catalysts scraped from the catalyst layer supported on Cu grids (300 mesh). High resolution TEM (HR-TEM) was conducted on a FEI Talos F200 TEM with accelerating voltage 200 kV. Thermogravimetric analysis (TGA) analysis was per-formed to 1 cm^2 pieces of GDEs in air from 20 to 900 °C to estimate the Pt loading. X-Ray diffraction (XRD) was run on a Bruker D8 Auto-sampler with a Cu $K\alpha$ X-Ray source (λ = 0.15406 nm) between 2θ values of 5-90° with a step size of 0.02° and dwell time of 0.47 s. X-ray

photoelectron spectroscopy (XPS) analysis was performed on a Thermo Fisher Scientific NEXSA spectrometer. The samples were analysed using a micro-focused monochromatic Al Kα source (72 W) over an area of approximately 400 microns. Charge neutralisation of the sample was achieved using a combination of both low energy electrons and Ar ions. All the data analysis was performed on the CasaXPS software (version: 2.3.18PR1.0) and sample charging corrected using the C 1s peak at 284.5 eV as reference. The pore size distributions of the as-prepared electrodes were determined using a mercury porosimeter (AutoPore IV, Micromeritics).

2.5. MEA fabrication and single cell testing

For Pt/N-CNT electrodes, 91.4 μL 10 wt% Nafion® solution (0.6 mg cm^{-2}) in 0.2 mL IPA was sonicated using a sonic bath for 5 min. before painting onto the electrode surface. The GDEs were then hot pressed to Nafion 212 membrane with the ionomer coated JM GDEs as anodes at 135 °C for 2 min. under an 1800 lb load. Benchmark GDEs were prepared from TKK Pt/C catalysts. Typically, a catalyst ink was made by dispersing a mixture of 13.9 mg Pt/C (TKK), 0.5 mL IPA and 91.4 μL Nafion® solution (10 wt%) by sonication horn (130 W, 20 kHz for 10 min. at 20% power). The ink was then painted onto a 16 cm^2 Sigracet 39 BC and left to dry at room temperature.

A PaxiTech-Biologic FCT-50S (Grenoble, France) PEMFC test stand was used for all single cell performance tests and electrochemical im-pedance spectroscopy (EIS) measurements. CV cycles and H$_2$ crossover measurements were run using an integrated EZStat-Pro, NuVant Systems Inc., USA. Polytetrafluoroethylene (PTFE) gaskets with thick-ness 254 μm were used for a gas seal at both the anode and cathode. The membrane was hydrated by holding the cell at 0.6 V for at least 10 h with cathode/anode conditions of fully humidified air/H$_2$ at 1.5 bar/ 1.5 bar absolute pressure and 1.5/1.3 stoichiometric coefficient. Break in and polarization curves were obtained with the cathode/anode fed with air/H$_2$ at 2.3 bar/2.5 bar absolute pressure and 1.5/1.3 stoichio-metric coefficient at 30%/50% relative humidity (RH), using the EU harmonized procedure. (G)EIS at 30 mA cm^{-2} and (P)EIS at 0.65 V and 0.5 V were recorded between 10 kHz-0.1 Hz with an amplitude of 72 mA, 10 mV and 10 mV, respectively.

For the kinetic characterization the cathode was fed with O$_2$ as the oxidant gas, and the stoichiometric coefficient was changed for the cathode/anode to 9.5/2, and the absolute pressures changed to 1.5 bar/ 1.5 bar respectively. The real impedance at the high frequency is taken as the uncompensated resistance for iR correction. To measure the parasitic H$_2$ crossover current, with the cathode being fully saturated with N$_2$, the potential was held at 0.5 V for 30 min. and the final current recording was taken. Cycle voltammetry (CV) analysis was run between 0.05–1.2 V vs. RHE at 20 mV s^{-1} with N$_2$ at the cathode. 3 cycles were recorded and the final one was used for electrochemical surface area (ECSA) calculation. To evaluate the durability of the cathodes, ac-celerated stress test (AST) was performed with 3000 potential sweeping cycles between 0.6–1.2 V at a scan rate of 100 mV s^{-1}. The ECSA values before and after the AST were used for comparison.

3. Results and discussion

3.1. Physical characterisation

In order to fabricate high performance electrodes for use in PEMFCs, CNTs were grown on a commercial Sigracet 39BC GDL via PECVD and subsequently nitrided using ASP treatment. Surface SEM images of the plain GDL and N-CNT GDL are shown in Fig. 2. The GDL surface mainly consists of carbon nanospheres at about 30–50 nm forming aggregates of 100–500 nm. Sigracet 39BC GDL also contains 5% PTFE coated on carbon nanospheres to prevent water flooding in practical operation. Fig. 2c and d show the GDL surface after the deposition of N-CNTs. It can be seen that N-CNTs form a thin porous layer on the surface, and
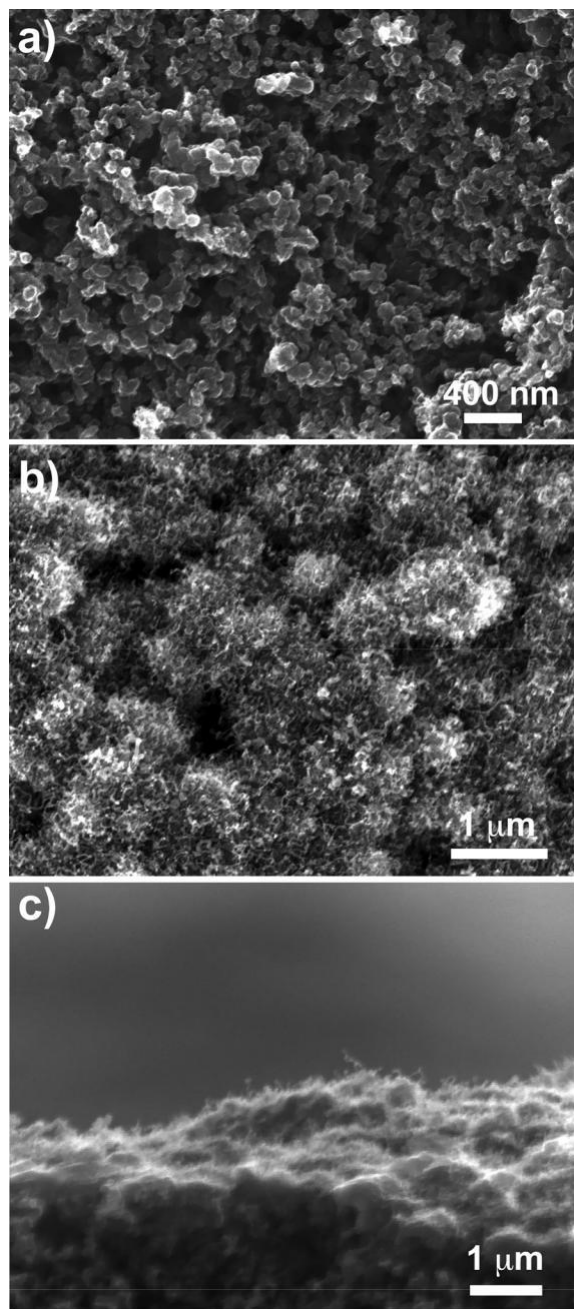

Fig. 2. Surface SEM images of (a) 39BC GDL and (b and c) N-CNT GDL. (c) shows the cross-section image of the N-CNT GDL.

the surface profile of the GDL is remained on the whole. N-CNTs are not highly ordered, but generally pointing out with an aligned structure.

TEM analysis was performed to observe the Pt/N-CNT nanos-tructures scraped from the GDE and the images are shown in Fig. 3. Entwined multiwall N-CNTs have an average diameter of ca. 10–20 nm and lengths of hundreds of nanometers. Some have an irregular nano-tube morphology. This is the same to the former report by a PECVD approach [25]. The nitriding provides the CNT surface with many de-fects which then act as required sites for Pt nucleation in the following Pt growth [28], leading to uniformly covered short Pt nanorods on the surface. The Pt nanorods have a diameter ca. 3–4 nm and lengths up to 10 nm. This ultrathin diameter is also ascribed to the defects formed by N doping on the CNT surface, confining the Pt atoms in reaction solu-tion to generate tiny nanoseeds thus inducing the following growth to achieve ultrathin 1D nanorods [31,32]. The length is shorter compared
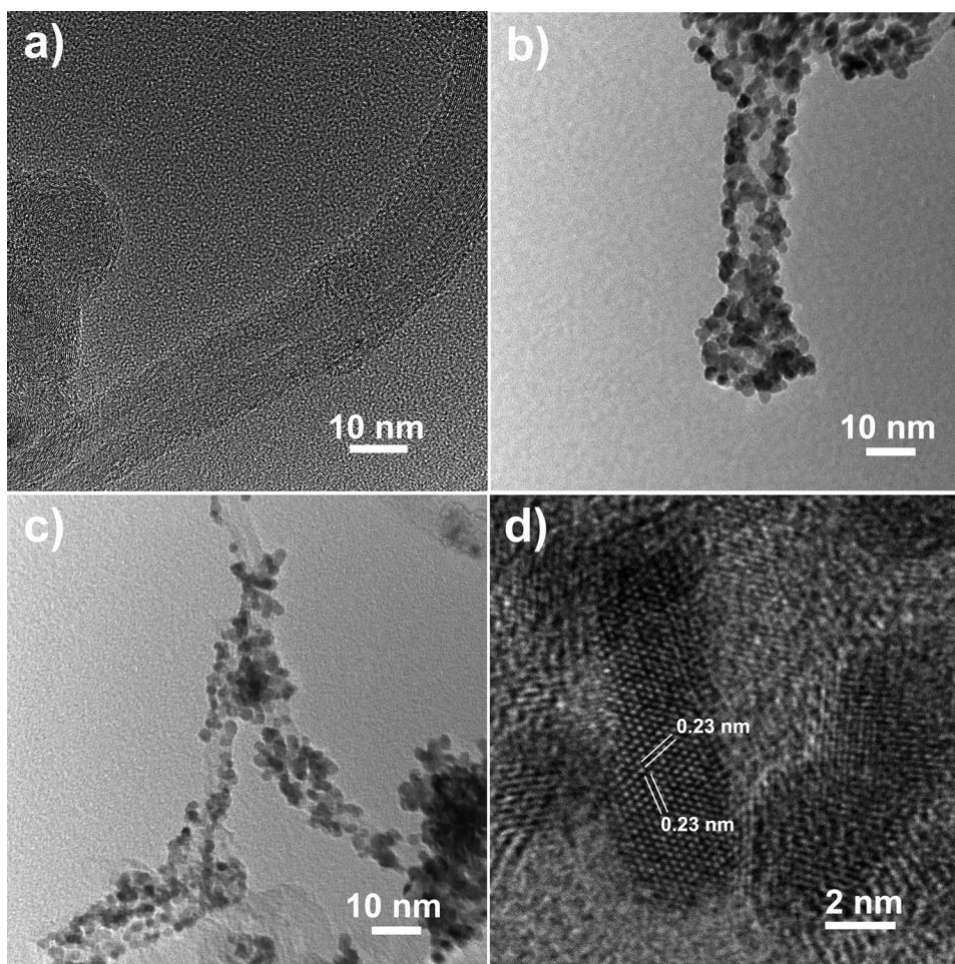
Fig. 3. (a) TEM images of N-CNTs supported on GDL surface and (c,d) Pt/N-CNTs scraped off the GDE surface, (d) HR-TEM images of Pt nanorods demonstrating the inter-lattice spacing of single crystal Pt nanorods growing along < 111 > direction.

with those obtained in room temperature but agree with our early work obtained at 40 °C [27]. The HR-TEM analysis (Fig. 3d) confirms the single crystal structures of these Pt nanorods growing along < 111 > direction. An inter-lattice spacing of 0.23 nm is observed consistent with the (111) plane and thus demonstrating highly ordered crystal-linity and preferential growth along the < 111 > direction, promoted by the use of HCOOH as the reducing agent [33].

TGA analysis (Fig. S2) indicates Pt loadings of 0.41 mg cm^{-2} and 0.19 mg cm^{-2} for Pt/C and Pt/N-CNT GDEs, respectively. Such a low Pt loading brings some difficulties for XRD analysis. XRD patterns of Pt/C, N-CNT/39BC and Pt/N-CNT GDEs are compared in Fig. 4a. Although all Pt peaks can still be indexed (JCPDS-04-0802), the intensity is very weak due to the very low Pt content. Notably Pt peaks are better de-fined for the Pt/N-CNT sample compared to the Pt/C demonstrating a higher crystallinity of Pt within nanorods. With N-CNT/39BC, the peaks in the 2θ range 12-25° are indexed to amorphous carbon and the dis-tinctive peak at 26.6° is for (002) of graphitic carbon [34].

XPS was conducted on the surface of the GDEs and a survey scan of the Pt/N-CNT GDE is displayed in Fig. 4b. The nitriding of the CNT structure is confirmed by the N1 s spectrum (Fig. 4c) observed for N-CNT/39BC (data shown in Table S1). The N1 s peak are fitted with assigned characteristic peaks for pyrridinic (398.1 eV), pyrrolic (399.4 eV), quaternary (400.8 eV) and pyridinic N-oxide (403.4 eV) [13,35]. Quaternary and pyrrolic N dominate the spectrum for N-CNT/ 39BC, but after the growth of Pt onto the N-CNT surface (Fig. 4c bottom), pyridinic N with the addition of M-N peaks (397.2 eV) be-comes more prominent. While it has been shown that Pt deposition

occurs on the hetero-atom dopants or on defects induced by such do-pants [36], the increase in pyridinic N here suggests that the Pt growth induces defects themselves thus promoting further nucleation. As a result nanorod sizes remain small and extended nanowire structures as seen from Pt reduction with formic acid on amorphous carbon are not observed [26]. Fig. 4d compares Pt4f scans of Pt/C and Pt/N-CNT, and the intensity of the peaks for the Pt/N-CNT GDE is much higher, in-dicating that most of the Pt present within the electrode is at the surface corresponding well with the SEM analysis above (Fig. 2). From the Pt4f region the Pt on Pt/N-CNT is composed almost entirely of Pt(0), whereas the Pt on Pt/C is composed of 56 atm% Pt(0), 34% Pt(II) and 10% Pt(IV) suggesting that the N-doped support reduces the Pt-O bond strength in relation to conventional supports. A small Pt(0) 7/2 peak shift of around 0.25 eV to lower binding energies is also observed for the Pt/N-CNT GDE compared to the Pt/C GDE, indicating an increased electron density on the Pt, transferred from the N-CNT support [36].

3.2. Electrode performance

To assess the performance of the Pt/N-CNT GDE under realistic operating conditions for automotive applications, polarisation curves and EIS spectra were obtained under the harmonised EU testing pro-tocol and are shown in Fig. 5. At the conventional fuel cell operational voltage 0.6 V, the power outputs obtained for the Pt/C and Pt/N-CNT GDEs are 0.442 and 0.544 W cm^{-2}, respectively. Despite a much lower Pt loading with the Pt/N-CNT electrode, a 1.23 fold increase in power output is achieved here. The comparison of EIS patterns at a low current
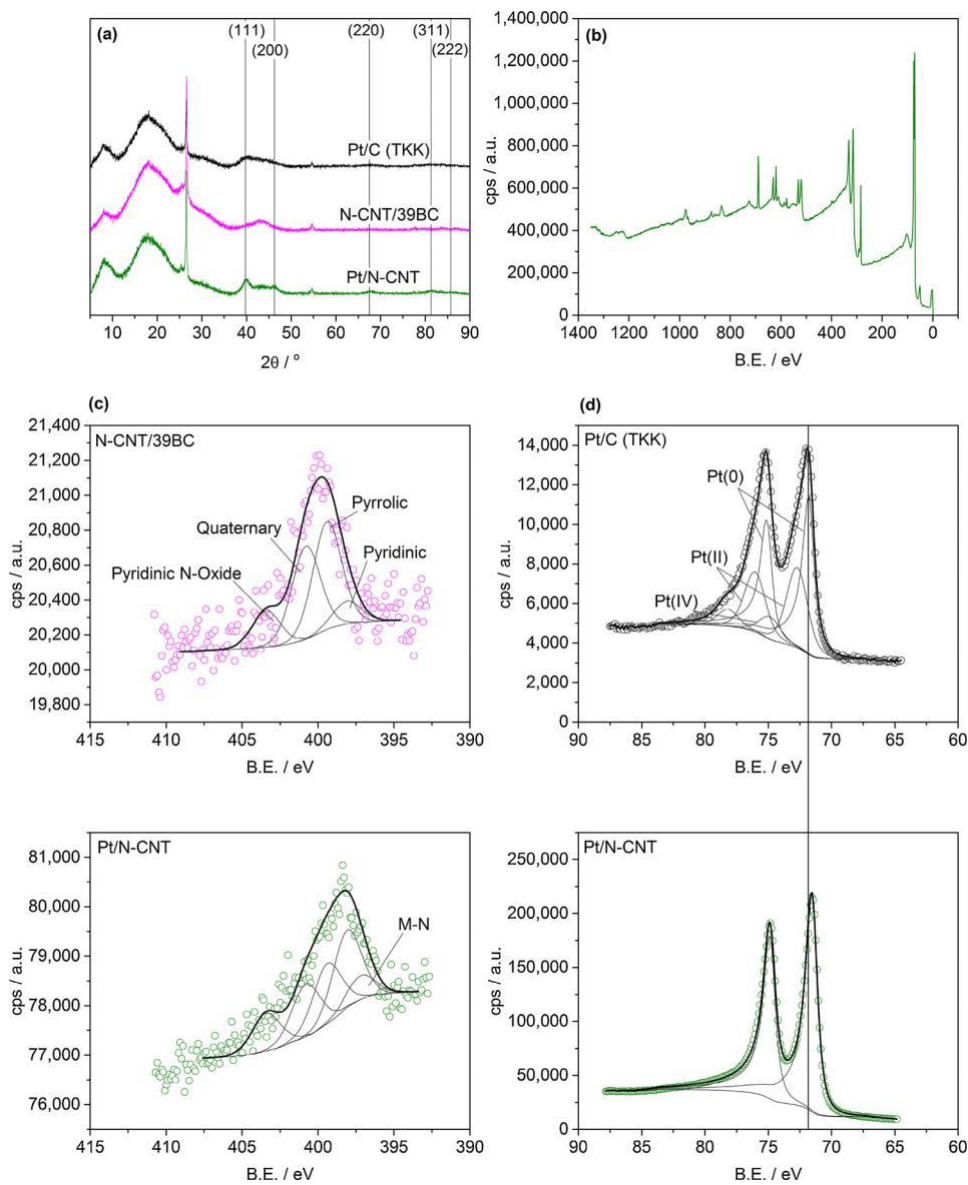
Fig. 4. (a) XRD spectra for the Pt/C GDE, N-CNT/39 BC GDL and Pt/N-CNT GDE. (b) XPS survey for the Pt/N-CNT GDE. (c) N1 s XPS spectra for N-CNT/39BC (top) and Pt/N-CNT (bottom) GDEs. (d) Pt4f XPS spectra for Pt/C (top) and Pt/N-CNT (bottom) GDEs. The vertical line indicates the Pt peak shift of around 0.25 eV.

density of 30 mA cm^{-2}, corresponding to a high voltage (Fig. 6b) exhibit close semicircles for both samples, indicating similar charge transfer resistance and kinetic activities. However the EIS spectra at high current densities/low voltages, 0.65 and 0.5 V, shows that besides from the lower semicircle at the high frequency range for the Pt/N-CNT GDE due to the improved ORR kinetics, a much smaller semicircle at the low frequency range reveals significantly reduced mass transport loss for the Pt/N-CNT GDE as compared to the Pt/C GDE, potentially resulting from the thin open catalyst layer.

To further understand the enhanced power performance of the Pt/ N-CNT GDE, ECSA and mass activities were obtained with MEA test in single cells. Cathode CVs of both electrodes are shown in Fig. 6a and the ECSA for the Pt/C electrode is calculated as 40.1 m^2 g$_{Pt}^{-1}$ (using the hydrogen desorption for the charge transferred and following the cal-culation method described well by Garsany et al. [37]). For Pt/N-CNT, the calculated ECSA is 21.9 m^2 g$_{Pt}^{-1}$. The lower ECSA for Pt nanorods results from their 1D nanostructure, which is also close to the value reported by our group before [31]. The mass activities from MEA test under O$_2$ was carried out following standard DOE protocol considering an iR and H$_2$ crossover corrections using the method detailed by

Gasteiger et al. [38]. Fig. 6b shows the original and corrected polarisation curves for the MEAs tested under O$_2$. The lower ECSA together with a lower Pt loading for the Pt/N-CNT GDE results in a slightly lower open circuit potential (OCP), which is as expected. Despite this initial efficiency loss for the Pt/N-CNT electrode, potential losses are smaller for Pt/N-CNT at currents greater than 0.2 A cm^{-2}. The mass activities calculated from the corrected polarisation curves at 0.9 V are 0.065 and 0.060 A/mg for Pt/N-CNT and Pt/C electrodes, respectively. A lower Tafel slope for Pt/N-CNT (44 mV dec^{-1}) compared to Pt/C (69 mV dec^{-1}) is also observed from the corrected polarisation curves. The transition of Tafel slope for Pt/C to higher values at higher over-potentials are often attributed to a decrease in Pt oxide coverage [39,40], however in the low over-potential region differences in Tafel slope are attributable to a difference in the rate determining step for the reaction [41]. One possibility is the reduced susceptibility to Pt oxide formation in the Pt/N-CNT catalyst as compared to the Pt/C (TKK) catalyst as evidenced both by the Pt4f XPS (Fig. 4d) and the more positive redox potential for PtO formation and reduction in the CV (Fig. 6a), which shifts the rate determining step away from the O$_2$ dissociation. Lower Tafel slopes have however been reported in previous reports of thin film
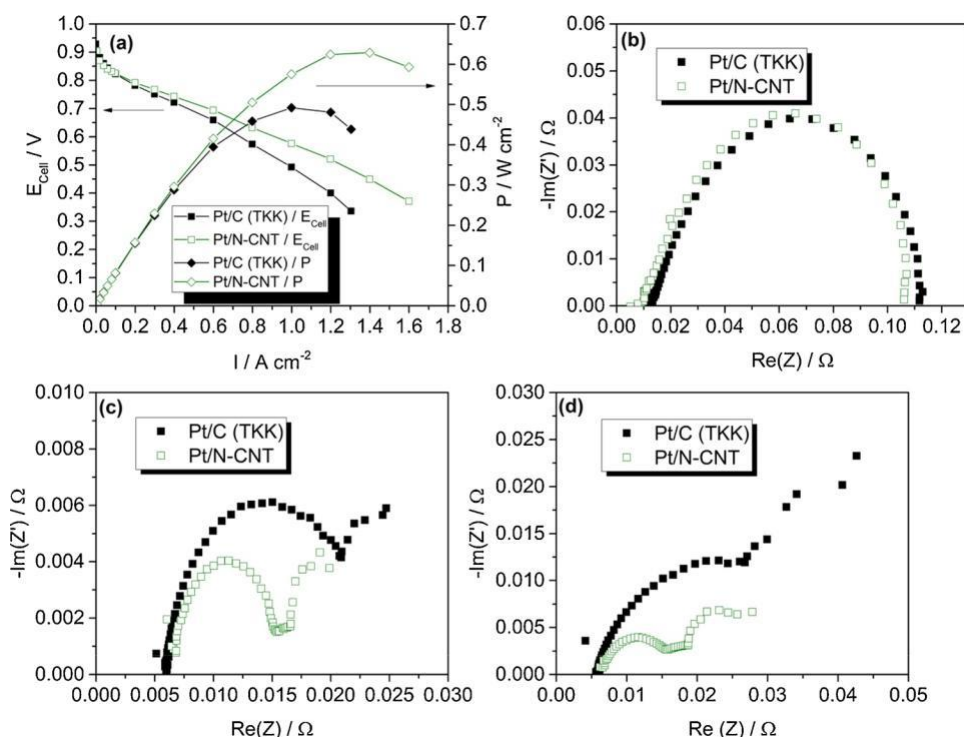
Fig. 5. Polarisation and power density curves (a), and Nyquist plots from EIS analysis in the frequency range 10 kHz – 0.1 Hz at (b) 30 mA cm^{-2}; (c) 0.65 V and (d) 0.5 V for the Pt/C and Pt/N-CNT GDEs under cathode/anode operating conditions of air/H$_2$, 1.5/1.3 stoichiometric flow, 2.3 bar/2.5 bar, 30%/50% RH at 80 °C.
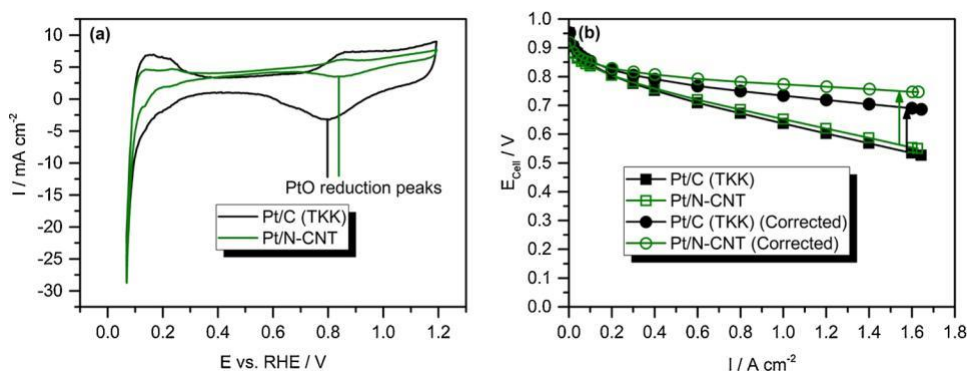

Fig. 6. (a) Cathode CVs of the Pt/C and Pt/N-CNT GDEs. (b) original uncorrected and corrected H$_2$/O$_2$ performance of the MEAs of the Pt/C and Pt/N-CNT GDEs. Measurements were taken at 80 °C with fully humidified reactants at 1.5 bar (H$_2$/O$_2$ stoichiometric flows of s = 2/ 9.5). The resistance-corrected cell voltage was determined via in situ EIS (evaluated at the high frequency) vs. current density. Current densities were H$_2$ crossover corrected to yield the shown effective current density.

catalyst layers and lower Pt loadings [27,42,43], and so the evidence suggests that asides from material composition, the catalyst layer structure has a considerable role in the kinetics of the ORR reaction that needs to be much better understood because of the clear impact that it has on the overall fuel cell performance.

The improved mass transport properties of the Pt/N-CNT can in part be ascribed to the reduced catalyst layer thickness, in which the catalyst is closer to the PEM results in a smaller migration path of the protons and hence a smaller proton transport resistance. Analogously with re-gards to gaseous transport, a decrease in mean free path due to thinner catalyst layer also results in faster reactant mass transport.

Alongside catalyst layer thickness, the porosity of the catalyst layer also has consequences for the mass transport resistance in operating PEMFCs. While large pores in the catalyst layer are best kept hydro-phobic for effective product removal and reactant transport, the small pores benefit from an increased proton transport with wettability. For example, replacing the conventional Nafion ionomer with the short side chain Aquivion ionomer has been shown to enhance PEMFC performance by being unable to penetrate the small pores and hence these regimes retain the natural hydrophobicity of the support [44].

As shown in the SEM images (Fig. 2), the aligned Pt/N-CNT catalyst layer shows a protruding structure of nanotubes which visibly in-creases the penetration of Nafion ionomer into the catalyst layer and hence an increase in proton transport is expected to be a source of improved PEMFC performance. A comparison of the pore size dis-tribution for Pt/C (TKK) and Pt/N-CNT GDEs is conducted based on the data obtained by mercury porosimetry analysis (Fig. S4). The pore size distribution of the Pt/C electrode shows an intense peak at ca. 100 nm which is very low for the Pt/N-CNT electrode, confirming the enhanced openness of the Pt/N-CNT electrode structure. Although thin film electrodes are reported to be susceptible to flooding, no is-sues were found for the Pt/N-CNT GDE as a result of a lack of non-noble cations which can increase the hydrophilicity of the catalyst surface [45] and the overall hierarchical structure of the catalyst layer [46]. While an assessment on the influence of pore size distribution is the objective of a future study however, it is clear that the improved performance of the Pt/N-CNT GDE in comparison to the Pt/C GDE is attributable to the unique catalyst layer structure afforded by the CNT support.
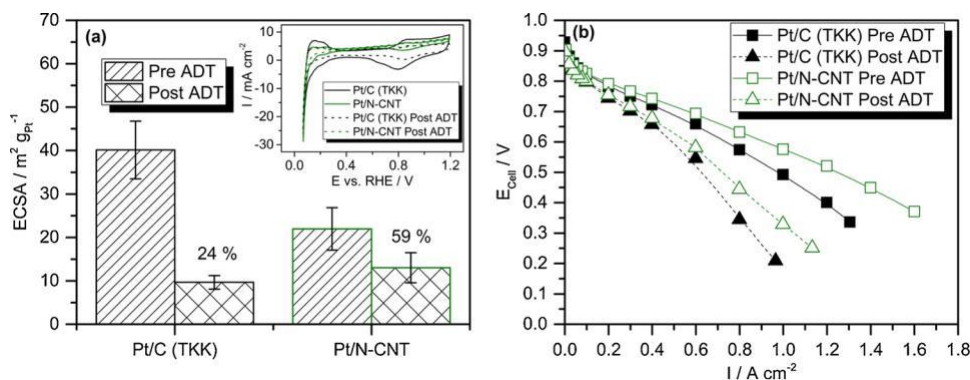
Fig. 7. (a) ECSA and (b) polarisation curve comparison for the Pt/C and Pt/N-CNT GDEs before and after the AST. The insert in (a) shows the CVs in the range 0.05–1.2 V vs. RHE.

3.3. Accelerated stress testing

Pt supported on N-CNTs have been reported to show improved stability compared to Pt/C catalysts after AST tests, attributed primarily to the improved carbon corrosion resistance of CNTs compared to mesoporous carbon [47]. Furthermore, 1D single crystal nanostructures also possess a better stability compared to their nanoparticle counter-part as electrocatalysts due to the special surface properties [48,49]. This work provides further evidence for these because after 3000 AST cycles at the high potential range (0.6–1.2 V vs. RHE) at the operation temperature, the Pt/N-CNT electrode shows a much smaller surface area loss of 41% compared to a 76% decrease for Pt/C (Fig. 7a), de-monstrating a higher stability of the Pt/N-CNT catalyst in MEAs. The power density of the MEAs after the AST was also tested for both samples. A higher power performance is also obtained for the MEA with the Pt/N-CNT GDE, 0.339 W cm^{-2} at 0.6 V over 0.308 W cm^{-2} for Pt/C (Fig. 7b). But, comparing to a much less ECSA loss in AST, the power density decline for the Pt/N-CNT GDE is 38%, higher than 30% of the Pt/C GDE. Considering the better stability of the catalyst, this is po-tentially caused by the electrode structure degradation due to the dif-ferent surface contact of Nafion electrolyte ionomer with nanowires as compared to with nanoparticles, which has also been reported by our and other research groups [48].

4. Conclusions

We have demonstrated direct fuel cell electrodes with a catalyst layer from Pt nanorods supported on N-doped CNTs. The direct deposition of CNTs by PECVD on GDLs forms a thin catalyst layer with open structure leading to a much improved mass transfer performance. The ASP treat-ment successfully nitrided the CNT surface providing nucleation cites for the in-situ growth of uniform highly active ultrathin Pt nanorods, finally delivering a larger mass activity. Both factors finally lead to a high power performance in H$_2$/air fuel cells. Furthermore, the Pt/N-CNTs exhibit a lower ECSA decline over Pt/C even after the durability test in PEMFCs due to the high stability of CNTs and Pt nanorods, showing a higher power performance but a slightly larger degradation percentage which can potentially be ascribed to the degenerate electrode structure caused by the poor contact between electrolyte ionomer and nanorod catalysts. Considering the easy scalability of PECVD, ASP and in-situ growing methods, therefore there is much promise for this electrode fabrication approach to produce very high performance electrodes after a further research to address the interface behaviour between catalyst and io-nomer for long-term applications.

Acknowledgements

Appendix A. Supplementary data

.

References

[1] A. Kongkanand, M.F. Mathias, The priority and challenge of high-power perfor-mance of low-platinum proton-exchange membrane fuel cells, J. Phys. Chem. Lett. 7 (2016) 1127–1137, https://doi.org/10.1021/acs.jpclett.6b00216.

[2] M. Shao, Q. Chang, J.-P. Dodelet, R. Chenitz, Recent advances in electrocatalysts for oxygen reduction reaction, Chem. Rev. 116 (2016) 3594–3657, https://doi.org/10. 1021/acs.chemrev.5b00462.

[3] M. Li, M. Li, Z. Zhao, T. Cheng, A. Fortunelli, C. Chen, R. Yu, L. Gu, B. Merinov, Z. Lin, E. Zhu, T. Yu, Q. Jia, J. Guo, L. Zhang, W.A.G. Iii, Y. Huang, X. Duan, Ultrafine jagged platinum nanowires enable ultrahigh mass activity for the oxygen reduction reaction, Science 9050 (2016) 1414–1419, https://doi.org/10.1126/science.aaf9050.

[4] B. Ifan, E. Lester, J. Rossmeisl, I. Chorkendorff, Toward sustainable fuel cells, Science 354 (2016) 1378–1380, https://doi.org/10.1126/science.aal3303.

[5] S. Sharma, B.G. Pollet, Support materials for PEMFC and DMFC electrocatalysts - a review, J. Power Sources 208 (2012) 96–119, https://doi.org/10.1016/j.jpowsour. 2012.02.011.

[6] R. Kou, Y. Shao, D. Wang, M.H. Engelhard, J. Hun, J. Wang, V.V. Viswanathan, C. Wang, Y. Lin, Y. Wang, I.A. Aksay, J. Liu, Enhanced activity and stability of Pt catalysts on functionalized graphene sheets for electrocatalytic oxygen reduction, Electrochem. Commun. 11 (2009) 954–957, https://doi.org/10.1016/j.elecom. 2009.02.033.

[7] H. Tang, J.H. Chen, Z.P. Huang, D.Z. Wang, Z.F. Ren, L.H. Nie, Y.F. Kuang, S.Z. Yao, High dispersion and electrocatalytic properties of platinum on well-aligned carbon nanotube arrays, Carbon 42 (2004) 191–197, https://doi.org/10.1016/j.carbon. 2003.10.023.

[8] A. Rubio, J.A. Alonso, P.M. Ajayan, Improved charge transfer at carbon nanotube electrodes, Adv. Mater. Commun. 11 (1999) 154–157, https://doi.org/10.1002/(SICI)1521-4095(199902)11:2<154::AID-ADMA154>3.0.CO;2-B.

[9] P. Luksirikul, K. Tedsree, M.G. Moloney, M.L.H. Green, Electron promotion by surface functional groups of single wall carbon nanotubes to overlying metal par-ticles in a fuel-cell catalyst, Angew. Chemie - Int. Ed. 51 (2012) 6998–7001, https:// doi.org/10.1002/anie.201201589.

[10] S. Du, Y. Lu, R. Steinberger-Wilckens, PtPd nanowire arrays supported on reduced graphene oxide as advanced electrocatalysts for methanol oxidation, Carbon 79 (2014) 346–355, https://doi.org/10.1016/j.carbon.2014.07.076.

[11] S. Du, Y. Lu, S.K. Malladi, Q. Xu, R. Steinberger-Wilckens, A simple approach for PtNi–MWCNT hybrid nanostructures as high performance electrocatalysts for the oxygen reduction reaction, J. Mater. Chem. A 2 (2014) 692, https://doi.org/10. 1039/c3ta13608f.

[12] R. Imran Jafri, N. Rajalakshmi, S. Ramaprabhu, Nitrogen doped graphene nano-platelets as catalyst support for oxygen reduction reaction in proton exchange membrane fuel cell, J. Mater. Chem. 20 (2010) 7114, https://doi.org/10.1039/ c0jm00467g.

[13] M.A. Molina-garcía, N.V. Rees, "Metal-free" electrocatalysis : quaternary-doped graphene and the alkaline oxygen reduction reaction, Appl. Catal. A Gen. 553 (2018) 107–116, https://doi.org/10.1016/j.apcata.2017.12.014.

[14] J. Zhang, PEM Fuel Cell Electrocatalysts and Catalyst Layers: Fundamentals and

Applications, Springer, London, 2008.

[15] Y. Chen, J. Wang, H. Liu, R. Li, X. Sun, S. Ye, S. Knights, Enhanced stability of Pt electrocatalysts by nitrogen doping in CNTs for PEM fuel cells, Electrochem. Commun. 11 (2009) 2071–2076, https://doi.org/10.1016/j.elecom.2009.09.008.

[16] K. Gong, F. Du, Z. Xia, M. Durstock, L. Dai, Nitrogen-doped carbon nanotube arrays with high electrocatalytic activity for oxygen reduction, Science 323 (2009) 760–764, https://doi.org/10.1126/science.1168049.

[17] H. Wang, M. Xie, L. Thia, A. Fisher, X. Wang, Strategies on the design of nitrogen-doped graphene, J. Phys. Chem. Lett. 5 (2014) 119–125, https://doi.org/10.1021/ jz402416a.

[18] S. Ratso, I. Kruusenberg, U. Joost, R. Saar, K. Tammeveski, Enhanced oxygen reduction reaction activity of nanotube catalysts in alkaline media, Int. J. Hydrogen Energy 41 (2016) 22510–22519, https://doi.org/10.1016/j.ijhydene.2016.02.021.

[19] J. He, X. He, L. Liu, B. Hu, F. Bai, P. Zhang, Tailoring carbon materials substrate to modify the electronic structure of platinum for boosting its electrocatalytic activity, J. Electrochem. Soc. 165 (2018) F247–F252, https://doi.org/10.1149/2.1041803jes.

[20] L. Zhang, Z. Xia, Mechanisms of oxygen reduction reaction on nitrogen-doped graphene for fuel cells, J. Phys. Chem. C 115 (2011) 11170–11176, https://doi.org/10.1021/jp201991j.

[21] K. Cheng, D. He, T. Peng, H. Lv, M. Pan, S. Mu, Porous graphene supported Pt catalysts for proton exchange membrane fuel cells, Electrochim. Acta 132 (2014) 356–363, https://doi.org/10.1016/j.electacta.2014.03.181.

[22] P. Mardle, O. Fernihough, S. Du, Evaluation of the scaffolding effect of Pt nanowires supported on reduced graphene oxide in PEMFC electrodes, Coatings 8 (2018) 48–56, https://doi.org/10.3390/coatings8020048.

[23] Z. Tang, C. Kok, K. Keat, Z. Tian, D.H.C. Chua, J. Lin, Enhanced catalytic properties from platinum nanodots covered carbon nanotubes for proton-exchange membrane fuel cells, J. Power Sources 195 (2010) 155–159, https://doi.org/10.1016/j. jpowsour.2009.06.105.

[24] J. Liu, Y. Yuan, G. Goenaga, D. Liu, Performance improvement of fuel cell using platinum functionalized aligned carbon nanotubes performance improvement of fuel cell using platinum functionalized aligned carbon nanotubes, NSTI-Nanotech. 3 (2010) 805–808.

[25] Y. Shen, Z. Xia, Y. Wang, C. Kok, J. Lin, Pt coated vertically aligned carbon nano-tubes as electrodes for proton exchange membrane fuel cells, Procedia Eng. 93 (2014) 34–42, https://doi.org/10.1016/j.proeng.2013.11.037.

[26] S. Du, A facile route for polymer electrolyte membrane fuel cell electrodes with in situ grown Pt nanowires, J. Power Sources 195 (2010) 289–292, https://doi.org/10.1016/j.jpowsour.2009.06.091.

[27] Y. Lu, S. Du, R. Steinberger-Wilckens, Temperature-controlled growth of single-crystal Pt nanowire arrays for high performance catalyst electrodes in polymer electrolyte fuel cells, Appl. Catal. B Environ. 164 (2015) 389–395, https://doi.org/10.1016/j.apcatb.2014.09.040.

[28] S. Sun, F. Jaouen, J.P. Dodelet, Controlled growth of Pt nanowires on carbon na-nospheres and their enhanced performance as electrocatalysts in PEM fuel cells, Adv. Mater. 20 (2008) 3900–3904, https://doi.org/10.1002/adma.200800491.

[29] R. Wang, D.C. Higgins, M.A. Hoque, D. Lee, F. Hassan, Z. Chen, Controlled growth of platinum nanowire arrays on sulfur doped graphene as high performance elec-trocatalyst, Sci. Rep. 3 (2013) 2431–2437, https://doi.org/10.1038/srep02431.

[30] S.C. Gallo, C. Charitidis, H. Dong, Surface functionalization of carbon fibers with active screen plasma, J. Vac. Sci. Technol. A. Vacuum, Surf., Film. 35 (2017) 21404–21413, https://doi.org/10.1116/1.4974913.

[31] S. Du, K. Lin, S.K. Malladi, Y. Lu, S. Sun, Q. Xu, R. Steinberger-Wilckens, H. Dong, Plasma nitriding induced growth of Pt-nanowire arrays as high performance elec-trocatalysts for fuel cells, Sci. Rep. 4 (2014) 1–6, https://doi.org/10.1038/ srep06439 6439.

[32] S. Sun, G. Zhang, Y. Zhong, H. Liu, R. Li, Ultrathin single crystal Pt nanowires grown on N-doped carbon nanotubes, Chem. Commun. 0 (2009) 7048–7050, https://doi.org/10.1039/b916080a.

[33] H. Meng, Y. Zhan, D. Zeng, X. Zhang, G. Zhang, F. Jaouen, Factors influencing the growth of Pt nanowires via chemical self-assembly and their fuel cell performance, Small 11 (2015) 3377–3386, https://doi.org/10.1002/smll.201402904.

[34] W. Ren, D. Li, H. Liu, R. Mi, Y. Zhang, L. Dong, L. Dong, Lithium storage perfor-mance of carbon nanotubes with different nitrogen contents as anodes in lithium ions batteries, Electrochim. Acta 105 (2013) 75–82, https://doi.org/10.1016/j. electacta.2013.04.145.

[35] S. Hou, X. Cai, H. Wu, X. Yu, M. Peng, K. Yan, D. Zou, Nitrogen-doped graphene for dye-sensitized solar cells and the role of nitrogen states in triiodide reduction, Energy Environ. Sci. 6 (2013) 3356–3362, https://doi.org/10.1039/c3ee42516a.

[36] J. Zhu, G. He, L. Liang, Q. Wan, P. Kang, Direct anchoring of platinum nanoparticles on nitrogen and phosphorus-dual-doped carbon nanotube arrays for oxygen re-duction reaction, Electrochim. Acta 158 (2015) 374–382, https://doi.org/10.1016/ j.electacta.2015.01.173.

[37] Y. Garsany, O. a Baturina, K.E. Swider-Lyons, S.S. Kocha, Experimental methods for quantifying the activity of platinum electrocatalysts for the oxygen reduction re-action, Anal. Chem. 82 (2010) 6321–6328, https://doi.org/10.1021/ac100306c.

[38] H.A. Gasteiger, S.S. Kocha, B. Sompalli, F.T. Wagner, Activity benchmarks and re-quirements for Pt, Pt-alloy, and non-Pt oxygen reduction catalysts for PEMFCs, Appl. Catal. B Environ. 56 (2005) 9–35, https://doi.org/10.1016/j.apcatb.2004.06. 021.

[39] M.K. Debe, Effect of electrode surface area distribution on high current density performance of PEM fuel cells, J. Electrochem. Soc. 159 (2012) B53–B66, https:// doi.org/10.1149/2.032201jes.

[40] N.P. Subramanian, T.A. Greszler, J. Zhang, W. Gu, R. Makharia, Pt-oxide coverage-dependent oxygen reduction reaction (ORR) kinetics, J. Electrochem. Soc. 159 (2012) B531–B540, https://doi.org/10.1149/2.088205jes.

[41] T. Shinagawa, A.T. Garcia-esparza, K. Takanabe, Insight on Tafel slopes from a microkinetic analysis of aqueous electrocatalysis for energy conversion, Nat. Publ. Gr. 5 (2015) 1–21, https://doi.org/10.1038/srep13801 13801.

[42] H.A. Gasteiger, J.E. Panels, S.G. Yan, Dependence of PEM Fuel Cell Performance on Catalyst Loading 127 (2004), pp. 162–171, https://doi.org/10.1016/j.jpowsour. 2003.09.013.

[43] A.E.S. Sleightholme, D.P. Wilkinson, D. Bizzotto, S. Ye, L. Gyenge, Nafion film-templated platinum electrodes for oxygen reduction, Electrocatalysis 1 (2010) 22–27, https://doi.org/10.1007/s12678-010-0006-1.

[44] Y. Garsany, W.A. Iii, M.B. Sassin, R.M.E. Hjelm, B.D. Gould, K.E. Swider-lyons, Improving PEMFC performance using short-side-chain low-equivalent-Weight PFSA ionomer in the cathode catalyst layer, J. Electrochem. Soc. 165 (2018) F381–F391, https://doi.org/10.1149/2.1361805jes.

[45] M.K. Debe, Electrocatalyst approaches and challenges for automotive fuel cells, Nature 486 (2012) 43–51, https://doi.org/10.1038/nature11115.

[46] Y. Zeng, Z. Shao, H. Zhang, Z. Wang, S. Hong, Nanostructured ultrathin catalyst layer based on open-walled PtCo bimetallic nanotube arrays for proton exchange membrane fuel cells, Nano Energy 34 (2017) 344–355, https://doi.org/10.1016/j. nanoen.2017.02.038.

[47] E. Antolini, Carbon supports for low-temperature fuel cell catalysts, Appl. Catal. B Environ. 88 (2009) 1–24, https://doi.org/10.1016/j.apcatb.2008.09.030.

[48] B. Li, D.C. Higgins, Q. Xiao, D. Yang, C. Zhng, M. Cai, Z. Chen, J. Ma, The durability of carbon supported Pt nanowire as novel cathode catalyst for a 1.5 kW PEMFC stack, Appl. Catal. B Environ. 162 (2015) 133–140, https://doi.org/10.1016/j. apcatb.2014.06.040.

[49] S. Sun, G. Zhang, D. Geng, Y. Chen, R. Li, M. Cai, X. Sun, A highly durable platinum nanocatalyst for proton exchange membrane fuel cells: Multiarmed starlike nano-wire single crystal, Angew. Chemie - Int. Ed. 50 (2011) 422–426, https://doi.org/ 10.1002/anie.201004631.